第 28 卷第 3 期
2012 年 3 月

无 机 化 学 学 报
CHINESE JOURNAL OF INORGANIC CHEMISTRY

Vol.28 No.3
601-606

硫辅助合成高孔隙率大孔氮化硼材料

孙常慧 徐立强* 马小健 钱逸泰
(山东大学胶体与界面化学教育部重点实验室,济南 250100)

摘要：采用硫粉辅助的方法合成了具有一定有序孔洞结构的三维大孔氮化硼材料，具有高比表面积 (230 $m^2 \cdot g^{-1}$) 和高孔隙率(85.6%),并呈现开孔结构。在未加入硫粉的情况下则只形成完全无序的三维大孔氮化硼,并且比表面积和孔隙率分别降至 122 $m^2 \cdot g^{-1}$ 和 73.7%。热重测试表明两种产品均具有良好的抗氧化性能。本文还对这种大孔材料的形成过程和硫粉的作用进行了初步的探讨。

关键词：氮化硼；大孔；孔隙率
中图分类号：O613.61；O613.8+1；O613.51 **文献标识码**：A **文章编号**：1001-4861(2012)03-0601-06

Sulfur-Assisted Synthesis of Highly Porous Macroporous Boron Nitride Materials

SUN Chang-Hui XU Li-Qiang* MA Xiao-Jian QIAN Yi-Tai
(*Key Laboratory of Colloid and Interface Chemistry, Shandong University, Ministry of Education, Jinan* 250100, *China*)

Abstract: Three-dimensional (3D) macroporous boron nitride materials with a certain order of pore arrangements have been synthesized in the existence of sulfur powders. The as-obtained materials exhibit open macropores with high specific surface area of 230 $m^2 \cdot g^{-1}$ and high porosity of 85.6%. Without addition of sulfur disordered 3D macroporous boron nitride was formed only and its specific surface area and porosity were decreased to 122 $m^2 \cdot g^{-1}$ and 73.7%, respectively. Both of the products obtained with and without addition of sulfur show good oxidation resistance below 800 ℃. The formation process and the role of sulfur powders were studied.

Key words: boron nitride; macroporous; porosity

0 Introduction

Recently, as a new porous material, three-dimensional ordered macroporous (3DOM) materials (pore size ranging from 50 nm to several micrometres) have been developed[1-3]. Their potential applications are envisioned in the realms of photonic band gap (PBG) materials, battery electrodes, catalytic supports, adsorbents, membranes for separation processes, and chemical sensors[4-9]. To date, almost all of the 3DOM metals, metal oxides and carbides have been synthesized by the general colloidal crystal (silica or polystyrene (PS) spheres) templating methods[10-12].

Boron nitride (BN) is a wide band gap Ⅲ-Ⅴ compound with remarkable physical and chemical properties, for example, high temperature stability, high oxidation and corrosion resistance, high thermal conductivity, and low dielectric constant. BN particles with various morphologies, such as tube, wire, platelet, whisker, sphere have been synthesized by arc discharge, laser ablation, carbothermal reduction, template-aided synthesis, chemical vapor deposition, and co-pyrolysis route[13]. The tremendous passion for porous materials has driven the development of boron

收稿日期:2011-06-23。收修改稿日期:2011-10-03。
国家自然科学基金(No.20871075 和 20971079),973 计划(No.2011CB935901)资助项目。
*通讯联系人。E-mail:xulq@sdu.edu.cn

nitride materials with different porous characteristics. In last decade, Smith Group[14] developed a series of microporous boron nitride via pyrolysis of polymeric precursors with different adsorption behaviors towards CH_4 and CO_2. Moreover, mesoporous boron nitride has been fabricated using different hard templates such as CMK-3, CMK-8 or SBA-15 and carbon-template substitution reaction from porous carbon[15-18]. Sung et al.[19] attempted to prepare 3DOM boron nitride using monodisperse colloidal silica spheres as template and failed to obtain the satisfaction results.

Herein, we report a facile single-source precursor approach to prepare highly porous macroporous boron nitride powders. The reaction was carried out in an autoclave via the pyrolysis of NH_4BF_4 with the presence of reduced Fe and S powders. Additionally, the reaction without the presence of S powders was also performed. Detailed comparison on the structure and performance of the two products was described.

1 Experimental

All the chemical reagents were of analytical-grade purity (Shanghai Chem. Co.) and were used without further purification. In a typical experimental procedure, NH_4BF_4 (50 mmol), Fe (80 mmol) and S (20 mmol) were mixed into a 25 mL stainless steel autoclave. The autoclave was then sealed and put into an electric furnace. The temperature of the furnace was increased from room temperature to 500 ℃ and maintained at 500 ℃ for 20 h. After the autoclave was cooled to room temperature naturally, the grayish white solid powders were collected and stirred vigorously in concentrated hydrochloric acid (3 mol·L^{-1}) for 12 h. Then, the solution was washed with ethanol and distilled water several times to eliminate the byproducts. Finally, the product was filtered and dried in a vacuum at 70 ℃ for 6 h. To eliminate residual S powders, the product was infiltrated in carbon disulfide for 1 h and then filtered. The as-obtained sample was denoted as BN_s (the subscript "s" represents "sulfur"). For the sake of comparison, the sample prepared without the presence of S powders by the same procedure was denoted as BN_{ws} (the subscript "ws" represents "without the presence of S powders").

X-ray powder diffraction (XRD) measurements were carried out using a Bruker D8 advanced X-ray diffractometer (Cu $K\alpha$ radiation of 0.154 18 nm, 40 kV, 40 mA, Ni filter, Scintillation counter). X-ray Photoelectron Spectroscopy (XPS) measurements were performed using Perkin-Elmer 5300 X-Ray Photoelectron Spectrometer with monochromatic Al radiation (λ=0.834 12 nm). Scanning electron microscope (SEM) images were taken with a JEOL JSM-6700F field emission electron microscope, in which the powders were directly deposited onto copper discs. High resolution transmission electron microscopy (HRTEM) images were recorded on a JEOL-2100 transmission electron microscope at an acceleration voltage of 200 kV. Nitrogen adsorption isotherms of the materials were determined using nitrogen in a conventional volumetric technique to characterize the meso- and/or micropores of the samples. Prior to the sorption measurements, the samples were degassed at 573 K under vacuum for 6 h. A mercury porosimeter (Autopore Ⅳ 9510, Micromeritics) was used to characterize the macropores of the samples. Thermal gravimetric analysis (TGA) was taken on a Mettler Toledo TGA/SDTA851 thermal analyzer apparatus in following air with a temperature ramp of 10 ℃·min^{-1}.

2 Results and discussion

The powder XRD patterns of the two samples are shown in Fig.1. Both of them exhibit relatively intense peaks at $2\theta \approx 26.7°$ and 26.6° for BN_{ws} and BN_s respectively, which can be indexed as the (002) reflection of the hexagonal BN (h-BN). The corresponding d_{002} spacing for sample BN_{ws} and BN_s is 0.333 nm and 0.335 nm, which conform to the d_{002} spacing for graphitic boron nitride of 0.333 nm (PDF No.34-0421). It is noteworthy that both the (002) reflections of sample BN_s and BN_{ws} shift towards lower angles with simultaneous slight broadening of the peaks (see the dashed line in Fig.1). This is probably due to lattice expansion between two adjacent BN slabs along the c-axis induced by the introduction of strain in the

bent layers[20]. No characteristic peaks associated with other crystalline materials were detected in the patterns suggesting high purity of two samples.

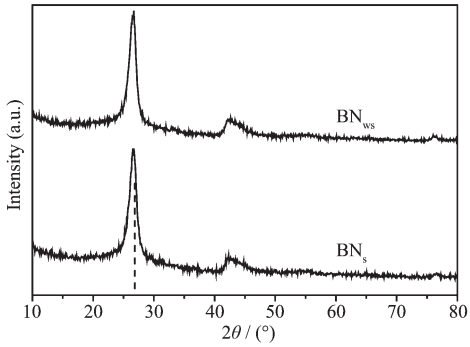

Fig.1　Typical XRD patterns of sample BN_{ws} and BN_s

XPS measurements were implemented to further interpret the chemical compositions of the as-prepared macroporous boron nitride materials. From the typical survey spectra of BN_{ws} and BN_s in Fig.2, both of the two samples contain N and B elements, while C and O signals can be attributed to the adsorption of CO_2, H_2O, or O_2 on the surface of the samples. The insets in Fig.2a and Fig.2b show the high-resolution N1*s* and B1*s* spectra. The binding energies centered at 398.2 eV for N1*s* and 190.5 eV for B1*s* in BN_{ws} and 398.2 eV for N1*s* and 190.4 eV for B1*s* in BN_s are in good agreement with the reported values for h-BN[21].

Morphological observations were conducted using SEM technique and the resulting images are presented in Fig.3. Both of the samples show polycrystalline structures from the SAED patterns (insets in Fig.3c and 3e). The highly porous and foamed surface of sample BN_{ws} analogous to wood can be clearly discerned from Fig.3a ~c. The pore size, however, estimated from the SEM images, displays a relatively wide distribution from 400 nm to 1 μm. For sample

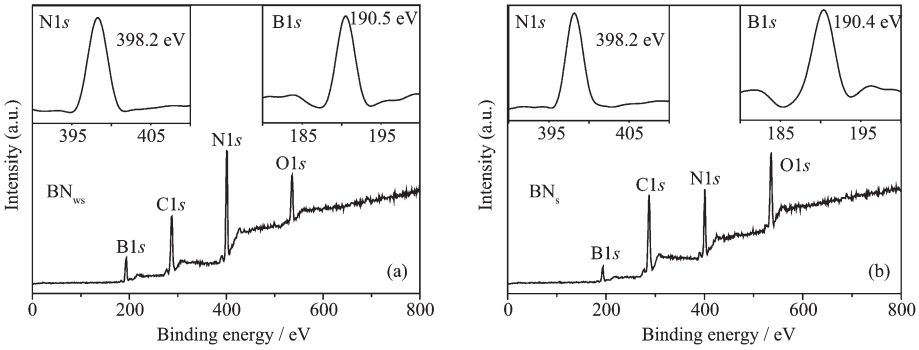

Fig.2　XPS spectra of sample (a) BN_{ws} and (b) BN_s

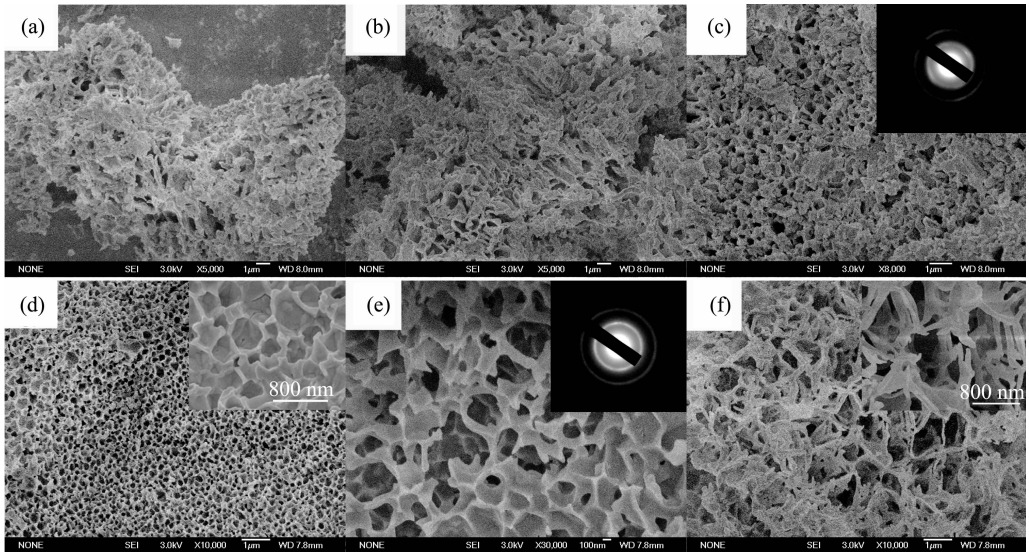

Insets in (c) and (e) show the selected area electron diffraction (SAED) patterns for samples BN_{ws} and BN_s; Insets in (d) and (f) show high resolution SEM images of sample BN_s

Fig.3　SEM images for samples (a~c) BN_{ws} and (d~f) BN_s

BN_s, a quite different pore appearance from BN_{ws} is demonstrated in Fig.3d~e. Almost all of the copious macropores exhibit open pore structure either restricted in closed channels (inset in Fig.3d) or interconnected forming 3D open network (Fig.3e). The pore structure and arrangement resemble somewhat that of the 3DOM metal oxides or carbon prepared by colloidal crystal templating method, albeit comparatively disordered and nonuniform[24-25]. The pore size mainly ranges from 200 to 400 nm and wall thickness lies from 20 to 40 nm. In addition, an unexpected peculiar fishbone-like architecture is found for the first time with negligible amount (Fig.3f). Overall, reduced pore size, increased porosity and more diversified pore texture make sample BN_s more attractive for wider promising applications.

The detailed pore characters of the samples were measured by a combination of nitrogen adsorption and mercury porosimetry. From the obtained nitrogen adsorption-desorption isotherms in Fig.4a and 4b, both are close to type-Ⅱ isotherm with a strong increase in adsorbed nitrogen volume at relative pressure (p/p_0) higher than 0.9, where the adsorption and desorption branches of the isotherm almost coincide to multilayer adsorption on a macroporous solid. The similar isotherms have often been observed in the reported macroporous materials[7,11]. Additionally, type H4 hysteresis loops are found in the relative pressure range of 0.3~0.9 for sample BN_{ws} and 0.1~0.9 for sample BN_s indicating the presence of textural mesopores within the wall structure and a pore size distribution extending to the macropore range[22]. In addition, Hg porosimetry was used to evaluate the various pore parameters including surface area, pore volume, porosity, and pore size distribution. The data are summarized in Table 1. Porosity was calculated by the amount of intrusion Hg in the macropore[23]. Fig.4c shows the pore size distributions measured by mercury porosimetry for the as-prepared samples. It can be found that sample BN_s possesses smaller pore size and narrower pore size distribution but larger pore volume than those of sample BN_{ws}. This can be interpreted by the higher porosity of sample BN_s as shown in Table 1. Obviously, the addition of S powders is proved to significantly improve the textural properties of the end products. Both of the samples exhibit relatively large surface area and pore volume comparable to previously reported microporous and mesoporous boron nitride materials [14-18]. Therefore, the obtained macroporous boron nitride materials have great advantage on the applications such as gas adsorption and catalyst supports[14,24].

Thermal stability and oxidation resistance of as-prepared macroporous boron nitride materials was estimated by TGA method from room temperature to 1 200 ℃ under flowing air. From the dashed curve for BN_{ws} in Fig.5, a slight weight loss of ~1.5% is observed before ~800 ℃ due to the removal of physi-

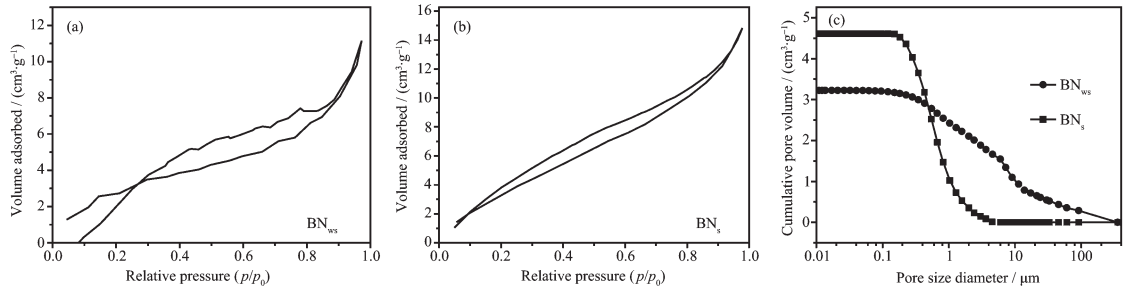

Fig.4 N_2 adsorption-desorption isotherms for sample (a) BN_{ws} and (b) BN_s (c) Pore size distributions measured by mercury porosimetry

Table 1 Pore characteristics of the samples from Hg porosimetry

Sample	Porosity / %	Surface area / ($m^2 \cdot g^{-1}$)	Pore volume / ($cm^3 \cdot g^{-1}$)	Average pore diameter / nm
BN_{ws}	73.7	122	0.32	917.3
BN_s	85.6	230	0.46	388.1

sorbed water or other atmosphere gases. However, when the temperature keeps increasing from ~800 to ~1 100 ℃, the sample BN_{ws} undergoes a rapid weight gain indicating the drastic oxidation of BN into B_2O_3. Compared with sample BN_{ws}, the TGA curve of sample BN_s (solid line in Fig.5) exhibits several different characters. Firstly, the weight loss before oxidation temperature reaches ~7.3% suggesting larger adsorption capacity of sample BN_s than BN_{ws}. Secondly, the onset oxidation temperature rises to ~900 ℃ which is higher than that of BN_{ws} and other reported boron nitride materials [20,25]. These distinct features reveal excellent structural stability against oxidation of macroporous BN_s indicating promising applications at high temperature and in rigorous environments.

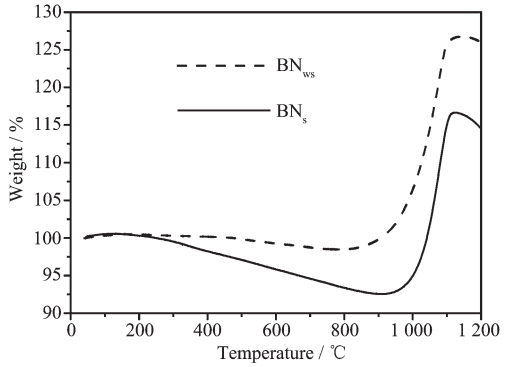

Fig.5　TGA curves of sample BN_{ws} (dashed line) and BN_s (solid line)

To understand the formation mechanism of macroporous boron nitride materials with a certain order by using S powders as additive, a series of relevant experiments were carried out through similar processes. Firstly, the effect of reaction temperature and time on the formation of macroporous boron nitride materials was investigated. It is found that lower temperature than 500 ℃ could not effectively initiate the reaction and higher temperatures resulted in large particles and flakes. Proper reaction time is also propitious to the formation of macroporous boron nitride materials and shorter time than 20 h leads to insufficient crystallization and vesicle-like particles with few porous structures. Apart from these, iron and S powders play a critical role in the formation of macroporous boron nitride materials. The reaction between NH_4BF_4 and Fe powders was studied previously using the same preparation methods and almost no porous structure was found at that time[26]. The difference here is that we double the dose of both the reactants, which leads to floppy macroporous boron nitride materials (i.e. BN_{ws}). This may indicate that the formation of porous boron nitride materials needs larger pressure and more Fe powders which act not only as catalyst but also as promoter or template for porous boron nitride materials. Additionally, for sample BN_s, when the amount of S powders is increased to 30 or even 50 mmol (No.1 and 2 in Table 2), the as-prepared product is composed mostly by large vesicles and/or flakes.

During the overall process, several reactions may be involved as follows:

$$NH_4BF_4 \rightarrow BF_3(g)+NH_3(g)+HF(g) \quad (\text{Ⅰ})$$

$$BF_3+NH_3 \rightarrow BN+3HF \quad (\text{Ⅱ})$$

$$2HF+Fe \rightarrow FeF_2+H_2 \quad (\text{Ⅲ})$$

$$Fe+S \rightarrow FeS \quad (\text{Ⅳ})$$

It is obvious that the reaction (Ⅱ) is a key process for the formation of macroporous BN materials, which is endothermic and can not be thermodynamically spontaneous according to the thermodynamic calculations (ΔH =116.7 kJ·mol^{-1}, ΔG =34.6 kJ·mol^{-1})[27]. While the reaction (Ⅲ) is exothermic and thermodynamically spontaneous (ΔH =−153.1 kJ·mol^{-1}, ΔG =−39.4 kJ·mol^{-1}), which greatly promotes the rightward process of the reaction (Ⅱ). The S vapor produced at high temperature may provide a transient driving force for rolling of the h-BN layers to form cavities of porous boron nitride materials [28]. Moreover, sulfur is believed to play a positive role in promoting the homogeneously mixing of reactants and in reducing the diffusion barriers, which leads to more complete reaction and more uniform morphology in shape and size. However, detailed information about the role of S powders is still incomplete and needs further investigation.

3　Conclusions

In conclusion, 3D macroporous boron nitride materials with a certain order were prepared by using NH_4BF_4 and Fe as reactants and S powders as additives. It is the auxiliary effect of S powders that

improves the textural and other properties of as-prepared macroporous boron nitride materials.

References:

[1] Holland B T, Blanford C F, Stein A. *Science*, **1998**,**281**:538-540

[2] Blanford C F, Yan H W, Schroden R C, et al. *Adv. Mater.*, **2001**,**13**:401-407

[3] Yuan Z Y, Su B L. *J. Mater. Chem.*, **2006**,**16**:663-667

[4] Subramanian G, Manoharan V N, Thorne J D, et al. *Adv. Mater.*, **1999**,**11**:1261-1265

[5] Esmanski A, Ozin G A. *Adv. Funct. Mater.*, **2009**,**19**:1999-2010

[6] Christian, Mitchell M, Kim D P, et al. *J. Catal.*, **2006**,**241**: 235-242

[7] Ma T Y, Zhang X J, Shao G S, et al. *J. Phys. Chem. C*, **2008**,**112**:3090-3096

[8] Mitchell D T, Lee S B, Trofin L, et al. *J. Am. Chem. Soc.*, **2002**,**124**:11864-11865

[9] Li Y Y, Cunin F, Link J R, et al. *Science*, **2003**,**299**:2045-2047

[10]Gao W, Xia X H, Xu J J, et al. *J. Phys. Chem. C*, **2007**,**111**: 12213-12219

[11]Li H N, Zhang L, Dai H X, et al. *Inorg. Chem.*, **2009**,**48**: 4421-4434

[12]Wang H, Li X D, Yu J S, et al. *J. Mater. Chem.*, **2004**,**14**: 1383-1386

[13]Sun C H, Yu H X, Xu L Q, et al. *J. Nanomater.*, **2010**: 163561

[14]Janik J F, Ackerman W C, Paine R T, et al. *Langmuir*, **1994**,**10**:514-518

[15]Dibandjo P, Bois L, Chassagneux F, et al. *Adv. Mater.*, **2005**,**17**:571-574

[16]Dibandjo P, Chassagneux F, Bois L, et al. *Microporous Mesoporous Mater.*, **2006**,**92**:286-291

[17]Rushton B, Mokaya R. *J. Mater. Chem.*, **2008**,**18**:235-241

[18]Vinu A, Terrones M, Golberg D, et al. *Chem. Mater.*, **2005**, **17**:5887-5890

[19]Sung I K, Kim T S, Yoon S B, et al. *Stud. Surf. Sci. Catal.*, **2003**,**146**:547-550

[20]Sun C H, Guo C L, Ma X J, et al. *J. Cryst. Growth*, **2009**, **311**:3682-3686

[21]Wagner C D, Riggs W M, Davis L E, et al. *Handbook of X-ray Photoelectron Spectroscopy*. Minnesota: Perkin-Elmer Corporation, **1979**.

[22]Li W C, Lu A H, Weidenthaler C, et al. *Chem. Mater.*, **2004**,**16**:5676-5681

[23]Sadakane M, Takahashi C, Kato N, et al. *Bull. Chem. Soc. Jpn.*, **2007**,**80**:677-685

[24]Lin L X, Li Z H, Zheng Y, et al. *J. Am. Ceram. Soc.*, **2009**, **92**:1347-1349

[25]Meng X L, Lun N, Qi Y Q, et al. *Eur. J. Inorg. Chem.*, **2010**:3174-3178

[26]Xu L Q, Peng Y Y, Meng Z Y, et al. *Chem. Mater.*, **2003**, **15**:2675-2680

[27]Speight J G. *Lange's Handbook of Chemistry*, 16*th ed.*. New York: McGraw-Hill, **2004**.

[28]Hao X P, Wu Y Z, Zhan J, et al. *J. Phys. Chem. B*, **2005**, **109**:19188-19190